High-resolution chemical patterns from negative tone resists for the integration of EUV patterns of metal-oxide resists with directed self-assembly of block copolymers

Running title: High-resolution chemical patterns from negative tone resists for EUV plus DSA

Running Authors: Lee et al.

Kyunghyeon Lee[1], Emma Vargo[2], Christopher Eom[1], Ricardo Ruiz[2], and Paul F. Nealey [1,3,a)]

[1]University of Chicago, Pritzker school of molecular engineering, Chicago, IL, 60637

[2]Lawrence Berkeley National Laboratory, Molecular Foundry, Berkeley, CA, 94720

[3]Argonne National Laboratory, Material Science Division, Lemont, IL, 60439

a) Electronic mail: nealey@uchicago.edu

Abstract

Extreme ultraviolet (EUV) lithography faces significant challenges in designing suitable resist materials that can provide adequate precision while maintaining economically viable throughput. These challenges in resist materials have led to printing failures and high roughness in EUV patterns, compromising the performance of semiconductor devices. Integrating directed self-assembly (DSA) of block copolymers (BCPs) with EUV lithography offers a promising solution because while the BCPs register to the EUV-defined chemical guiding pattern, the thermodynamically-determined structures of the BCPs automatically rectify defects and roughness in the EUV pattern. Despite the superior

resolution of metal-oxide EUV resists (MOR), their application to DSA is limited by the difficulty in converting them into chemical patterns that allow effective transfer of the rectified patterns of DSA films into inorganic materials. To address this challenge, this study introduces a novel strategy for fabricating chemical patterns using hydrogen silsesquioxane (HSQ), a high-resolution negative tone inorganic resist, as a model system for MOR. Initially, a sacrificial Cr pattern is generated from HSQ patterns via reactive ion etching. The sacrificial Cr pattern is converted into a chemical pattern by first grafting a water-soluble polyethylene oxide brush onto the substrate, then wet etching the Cr, and finally grafting non-polar polystyrene brushes. Assembling polystyrene-*block*-poly(methyl methacrylate) on these patterns results in structures oriented and registered with the underlying pattern, achieving 24 nm full-pitch resolutions. This approach has the potential to integrate MOR patterns into the DSA process, thereby enabling the generation of high-quality sub-10 nm patterns with high-χ BCPs.

I. INTRODUCTION

With the successful commercialization of extreme ultraviolet (EUV) lithography, the semiconductor industry implemented the largest jump in photon energy ever experienced[1, 2]. By utilizing EUV photons with a 13.5 nm wavelength, which have 14 times higher energy than the photons used in ArF lithography, EUV lithography achieves features down to sub-10 nm in a single process[1, 3]. This technology simplifies the manufacturing process by reducing the need for multi-step processes such as litho-etch-litho-etch[4] and self-aligned double patterning[5]. Despite these advancements, EUV lithography still faces challenges[6] arising from the trade-off between resolution, line roughness, and sensitivity of resist materials, often referred to as the RLS trilemma[7-9]. This issue is exacerbated by shot noise arising from the low photon count per dose and by non-uniformities within the patterning materials themselves at the molecular scale, leading to printing failures and high roughness in the resulting patterns, which severely impact the performance of semiconductor devices[8, 10].

Directed self-assembly (DSA) of block copolymers (BCPs) offers a promising solution to the challenges with precision in EUV lithography by rectifying imperfections in resist patterns[11, 12]. When lamellae-forming BCPs are assembled on chemically patterned surfaces, their domains tend to align accurately with the underlying pattern[13, 14]. The assembled structure of the BCPs, described by the natural period (L_0), volume fraction, and spatial fluctuation at the domain boundaries, is primarily encoded in the thermodynamic parameters of BCPs, such as the number of repeating units (N), the Flory-Huggins interaction parameter (χ), and the segregation strength (χN) [15, 16]. Therefore, the structures of BCPs can be decoupled from the quality of lithographically-defined chemical patterns,

achieving a pattern with reduced roughness and defects[17, 18]. Stoykovich et al. have demonstrated effective pattern rectification by DSA, incorporating polystyrene-*block*-poly(methyl methacrylate) (PS-*b*-PMMA) on chemical patterns designed with pre-programmed roughness fluctuations[12]. Pattern rectification by DSA not only improves the quality of patterns but also improves the lithographic process window with the potential to improve yield[19]. Intel has successfully employed this concept in EUV lithography[20]. PS-*b*-PMMA assembled on EUV-generated chemical patterns with a 26 nm full-pitch has been shown to improve line width roughness after selectively etching the PMMA domain, even at a 50% lower dose[20]. Even though PS-*b*-PMMA, the most frequently used material for DSA, has reached its phase separation limits at EUV-relevant dimensions due to its relatively low χ value[21], next-generation DSA materials with higher χ values have been developed for continuing the integration of DSA with EUV lithography[22-24].

Chemically and geometrically well-defined patterns are crucial for the DSA of BCPs because they offer precise control over domain orientation and lateral ordering of assembled domains[14, 25, 26]. These chemical patterns should be carefully designed with geometries commensurate with the microdomain width and pitch, L_0, of the BCPs, along with sufficient wetting contrast between the alternating guide stripes. Chemical patterns are traditionally generated by directly patterning a film of organic materials that is preferential to one block of the BCP. This strategy is facilitated by the Liu-Nealey (LiNe) flow, in which a cross-linked polymer mat is patterned with "top-down" lithography [25, 27]. The geometry of the pattern, such as the pattern period (L_s) and width of the guide stripe (L_w), is defined by transferring a topographic resist pattern via dry etching, while the wetting characteristics of the patterned underlayer are determined by the choice of

underlayer[25, 27, 28]. The success of this conventional strategy has been demonstrated by employing positive tone resists of polymeric materials, which provide sufficient resolution in traditional optical lithography and can be easily removed with organic solvents, maintaining the desired wetting properties of the underlayer[25-27].

In EUV lithography, metal-oxide resists (MORs) have demonstrated the highest resolution by leveraging the high EUV absorbance of metals and their small molecular size, as well as eliminating the need for photoacid generators[29, 30]. Tin-oxide-based resist materials, commercialized by Inpria, exemplify these advantages by achieving 10 nm lines and space patterns[31, 32]. As the resolution targets of EUV lithography continue to be refined, reaching down to 16 nm full-pitch with high-NA tools, these materials also face the challenges of the RLS trilemma[33, 34], necessitating pattern rectification by DSA. However, rectifying MOR EUV patterns by DSA is not straightforward due to difficulties in converting them into chemical patterns[35]. The conventional strategy of directly patterning preferential underlayers is ineffective for MOR patterns because their negative tone behavior and harsh removal conditions can significantly alter the geometry and chemistry of organic films. Alternative strategies have been explored to utilize MOR patterns directly on non-polar organic underlayers as guide stripes in chemical patterns, given that MOR patterns typically have an affinity for polar polymers[35-37]. Despite its potential, the remaining MOR patterns beneath the polar block present significant challenges in transferring the rectified patterns in DSA films into inorganic materials for semiconductor applications. Successful pattern transfer requires converting the DSA patterns into an etch mask for reactive ion etching (RIE), typically achieved by selectively removing the polar block of BCPs, such as PMMA in PS-*b*-PMMA, leaving the non-polar block (e.g., PS) to

serve as the etch mask[21, 38, 39]. However, when MOR patterns are used as guide stripes for the polar block, they remain in areas that should be unprotected by the etch mask, severely obstructing subsequent RIE. Even when the polar block is converted into an inorganic etch mask via sequential infiltration synthesis[40, 41], the imperfect geometry of the underlying MOR patterns persists, hindering the pattern transfer of the rectified DSA patterns. Furthermore, this approach lacks control over the surface properties of MOR guide patterns, as they are inherently determined by the characteristics of the MOR materials.

In this study, we demonstrate a novel strategy for creating chemical patterns entirely composed of polymer brushes using negative tone inorganic resists, aimed at the integration of high-resolution MOR EUV patterns with DSA for pattern rectification. Due to limited access to MORs and EUV exposure tools, line-and-space patterns of hydrogen silsesquioxane (HSQ) generated by e-beam lithography were utilized as a model system for MOR patterns. Starting with HSQ patterns on a Cr underlayer, we created sacrificial patterns of Cr lines with RIE. The Cr patterns were then transformed into chemical patterns by grafting polyethylene oxide (PEO) brushes onto both the Cr patterns and the interspatial areas, followed by removal of Cr with a wet etchant and finally grafting PS brushes onto the exposed Cr-etched regions. On the chemical patterns generated through this process, we successfully achieved DSA of PS-*b*-PMMA, with the assembled domains well-oriented and registered with the underlying patterns. This approach enabled DSA down to a 24 nm full-pitch resolution, which corresponds to the phase-separation limit of PS-*b*-PMMA. Given that MOR patterns can serve as effective etch masks for creating sacrificial Cr patterns, the process flow described in this work offers a pathway for rectifying imperfections in MOR EUV patterns through DSA.

II. EXPERIMENTAL

A. Materials

Polystyrene-*b*-poly(methyl methacrylate) block copolymer (PS-*b*-PMMA), hydroxyl-terminated polystyrene (PS-OH), and hydroxyl-terminated poly(ethylene oxide) (PEO-OH) were purchased from Polymer Source, Inc., and used as received. The number average molecular weight (Mn) and polydispersity index (PDI) of these polymers are listed in Table 1. The L_0 of PS-*b*-PMMA was determined by fingerprint patterns assembled on a neutral substrate modified with P(S-*r*-PMMA)-OH brush (M_n = 14.2 kg/mol, PDI = 1.16, f_{PS} = 51%) (as shown in Supplementary Material Figure S1). Cross-linkable polystyrene (X-PS) containing 4 mol% of 4-vinylbenzocyclobutene (BCB) was synthesized by reversible addition fragmentation chain-transfer (RAFT) polymerization as described elsewhere[42]. Before cross-linking, the X-PS had a Mn of ~14 kg/mol and a PDI of 1.12. The HSQ used as the e-beam resist in the patterning process was purchased from Dischem (H-SiQ). The HSQ solution was diluted from the original concentration (2 wt% in MIBK) to 1 wt% when necessary. Toluene, N-methylpyrrolidone (NMP), chloroform, chlorobenzene, and HF were purchased from Merck and Fisher Scientific. Chromium mask etchant CE-5M was purchased from Transene. Nanostrip, a commercially available stabilized piranha solution, was purchased from KMG Electronic Chemicals. The solvents and chemicals described here were used without further purification.

	Mn (g/mol)	f_{PS} (%)	PDI	L_0 (nm)
PS-*b*-PMMA	74,800	51	1.08	38.2
	42,000	50	1.18	26.6
	34,000	50	1.07	24.2
PEO-OH	2,000	-	1.09	-
	4,200	-	1.05	-
PS-OH	2,000	-	1.07	-
	6,000	-	1.05	-

Table 1. Description of polymers used in this study.

B. E-beam lithography of HSQ on Cr underlayer

A 5 nm thick Cr underlayer was deposited on a Si wafer with an Angstrom EvoVac Electron Beam Evaporator. X-PS was spin-coated from 0.1 wt% toluene onto the Cr underlayer, yielding a film with a thickness of 5 nm. The substrate was then annealed at 250 ℃ for 30 min to cross-link the X-PS. HSQ grating patterns with L_s of 24–38 nm were generated onto the Cr/X-PS stack with a Raith EBPG 5000+ E-beam writer. Following a prebake of the substrate at 180 ℃ for 5 min, a 20–30 nm layer of HSQ was applied by spin-coating. The resist-coated wafer was not baked. The exposure was performed with an acceleration voltage of 100 kV and a 300 μm aperture. The e-beam writing parameters for each grating pattern, including width of lines, beam current, beam step size, and dose, are listed in Table 2. The patterns were developed by immersing them in a salty developer (1% NaOH and 4% NaCl in water) for 20 s, followed by two consecutive 1 min rinses in deionized water.

Pattern period (L_s, nm)	Width of lines (nm)	Beam current (nA)	Beam step size (nm)	Dose (mC/cm^2)
24	1	0.15		100
26	2			80
36	8		1	23
37	8	1		24
38	10			18

Table 2. The writing conditions for HSQ patterns

C. Creation of Cr sacrificial patterns

HSQ patterns were transferred into a Cr underlayer through an RIE process with a chlorine and oxygen plasma (Cl_2/O_2 at 30/10 sccm, bias power of 25 W and inductively coupled plasma (ICP) power of 400 W, under a pressure of 10 mTorr). Subsequently, the HSQ patterns along with the residual X-PS layer were removed. This was accomplished by submerging the substrate in a 0.1 v/v% HF solution for 10 min to dissolve the HSQ patterns, and subsequently immersion in nanostrip at 120 ℃ for 20 min to remove the remaining X-PS layer. For 26 and 24 nm full-pitch gratings, the substrate was cleaned solely with nanostrip to avoid the detachment of Cr patterns due to undercutting by HF.

D. Conversion of Cr patterns into chemical patterns consisting of PEO-OH and PS-OH brushes

PEO-OH was spin-coated from a 2 wt% solution of chlorobenzene onto the samples, yielding a film ~50 nm in thickness. The substrate was then annealed at 230 ℃ for 30 min to graft the PEO-OH through a condensation reaction, resulting in a ~5 nm thick layer of PEO. Excess PEO-OH was washed away by sonication in chloroform for 5 min. Following this, the PEO-OH-grafted Cr patterns were etched by a wet etchant consisting of ceric ammonium nitrate and perchloric acid (Transene CE-5M) for 5 min. The residual PEO-OH brushes were subsequently cleaned by sonication in NMP at 80 ℃ for 10 min. Afterwards, hydroxyl-terminated PS-OH was spin-coated from a 1 wt% solution in toluene onto the samples, yielding a film with thickness of ~40 nm. The substrate was then annealed at 230 ℃ for 30 min to graft the PS-OH onto the areas where Cr was etched away. Excess PS-OH was then removed by sonication in toluene for 5 min. Blanket samples of a 5 nm thick Cr and bare Si substrate were prepared through the same process.

E. Assembly of block copolymer films

On both the chemically patterned substrate and the chemically homogeneous blanket substrates, PS-*b*-PMMA films were spin-coated from a 1 wt% solution in toluene, yielding a thickness of $1.25L_0$, and then annealed for 10–30 min at 250 ℃ under nitrogen.

F. Characterization

Scanning electron microscope (SEM) images were captured on a Zeiss Merlin high-resolution field-emission SEM with a 1.5 kV accelerating voltage at a working distance below 3.5 mm using the in-lens secondary electron detector. The image brightness and contrast were adjusted for presentation. Atomic force microscopy (AFM) was performed on a Bruker MultiMode 8 microscope. The wetting behavior of blanket substrates before and after the sequential grafting of brushes was determined by analyzing the topography (island or hole) of an assembled BCP film whose thickness was incommensurate with an integer multiple of L_0. A $1.25L_0$ thick film of PS-*b*-PMMA was assembled on these substrates, and the topography was observed with AFM. Water contact angle (WCA) measurements with deionized water were carried out at room temperature using a goniometer. A 5 μL drop of water was placed on the surface and the WCA was measured.

III. RESULTS AND DISCUSSION

Chemical patterns for DSA must satisfy the following two design criteria[13, 26]: First, they must possess a geometry and period that is commensurate with the thermodynamically stable structures of the microphase-separated BCP, minimizing the entropic penalty caused by the stretching or compression of BCP chains. Second, the two distinct surfaces in chemical pattern must selectively attract each corresponding block of BCPs, ensuring proper domain registration through sufficient enthalpic gain from favorable contact. These chemical patterns are designed as either line-and-space or dot array patterns depending on the natural structures of BCPs, such as lamellae or cylinders, respectively. In this study, we

focused on the line-and-space chemical patterns for the 1-to-1 DSA of lamellae-forming PS-*b*-PMMA.

The direct patterning of an organic film preferential to one block of a BCP has been employed as a robust strategy to create chemical patterns meeting these two design criteria. A representative process is illustrated in the top box of Figure 1. The process starts with the deposition of resist films onto the preferential underlayers, such as a self-assembled monolayer[25], a polymer brush[26], or a cross-linked polymer mat[27]. After photolithography or e-beam lithography, a topographic pattern of resist is generated on the underlayer, and its geometry is then transferred into the underlayer by a breakthrough etch using an oxygen plasma. The resist patterns protecting the remaining polymer patterns are removed with organic solvents, resulting in a pattern of underlayer "guide stripes". In this process, the geometry of the guides stripes is defined by the topography of the resist pattern after breakthrough etching, while their chemistry is determined by the choice of the underlayer. The use of positive tone polymeric resist (e.g. PMMA) facilitates the guide stripe in maintaining the preferential wetting characteristics throughout the process due to their easy removal in organic solvents. The contrast of the interfacial energy between the guide stripe and the interspatial region can be further engineered by modifying the interspatial region with a polymer brush[26, 27].

Employing the MOR in this direct patterning process has been hindered by two main challenges. First, due to their negative tone behavior[32], the areas protected by resist patterns, which will be converted into guide stripes in the direct patterning strategy, are directly exposed to photons or electrons during the lithographic process. The high-energy radiation during lithography can oxidize the organic underlayers, compromising the

wetting characteristics of the guide stripes[43, 44]. Second, the harsh removal conditions of the MORs , such as RIE[45] and the exposure to HF[46], make it difficult to preserve both the geometry and chemistry of the guide stripes. To address these challenges, we propose a new fabrication strategy utilizing sacrificial patterns, which can be effectively converted into a pattern of polymer brushes. This method prevents the polymer brushes, which constitute the chemical patterns, from being involved in the lithography and resist stripping steps. Due to the limited access to commercial MORs and EUV tools, we utilized HSQ resists, an EUV-compatible negative tone resist[47], patterned with e-beam lithography as a model system.

The schematic illustration in the bottom panel of Figure 1 shows the process flow of the proposed strategy. The process starts with the deposition of a thin Cr layer as a sacrificial material on a Si substrate, with an X-PS layer on top to promote adhesion of HSQ patterns. HSQ resist film is coated onto this Cr/X-PS stack and then is patterned into line-and-space patterns using e-beam lithography. The topographic HSQ patterns are transferred into the Cr underlayer by RIE. Subsequently, the HSQ patterns are removed by exposure to dilute HF, followed by piranha cleaning of residual X-PS between the HSQ and Cr. In contrast to the direct patterning strategy, the resulting Cr patterns are not used as guide stripes but are converted into chemical patterns by successive grafting of polymer brushes. Initially, a PEO-OH brush is grafted onto the patterned substrate. Due to the surface oxidation of both the Cr lines and interspatial area by the piranha solution, the PEO-OH brushes non-preferentially graft onto these areas through a condensation reaction of the reactive -OH end groups with the surfaces. By dissolving Cr with an aqueous wet etchant, the PEO-OH brush that is grafted onto the Cr patterns are removed by undercutting,

leading to line-and-space patterns of PEO-OH brush. Water-soluble PEO-OH brush is essential in this step because it can effectively penetrate the aqueous wet-etchant. Finally, by grafting the non-polar PS-OH brush onto the empty areas where Cr was wet-etched, chemical patterns composed of alternating PEO-OH and PS-OH guide stripes are generated. Because the Cr lines only serve as a sacrificial pattern that defines the geometry of the PEO-OH brush patterns and are then stripped, the proposed strategy avoids the oxidation of the polymeric guide stripes during the lithography step. Additionally, the relatively mild wet-etching of Cr helps the PEO-OH brush pattern to preserve its geometry and chemistry.

The material requirements for sacrificial patterns are as follows. First, it must exhibit good adhesion to the resist material after exposure and develop in the lithography step. Second, to transfer the resist pattern to the sacrificial layer, a dry etching chemistry with high contrast between the resist pattern and the sacrificial layer is necessary, and a strip chemistry must be available for the removal of resist patterns. Third, to effectively create PEO-OH brush patterns, the PEO-grafted underlayer must be easily removed by a wet etchant without damaging the PEO brush's chemistry.

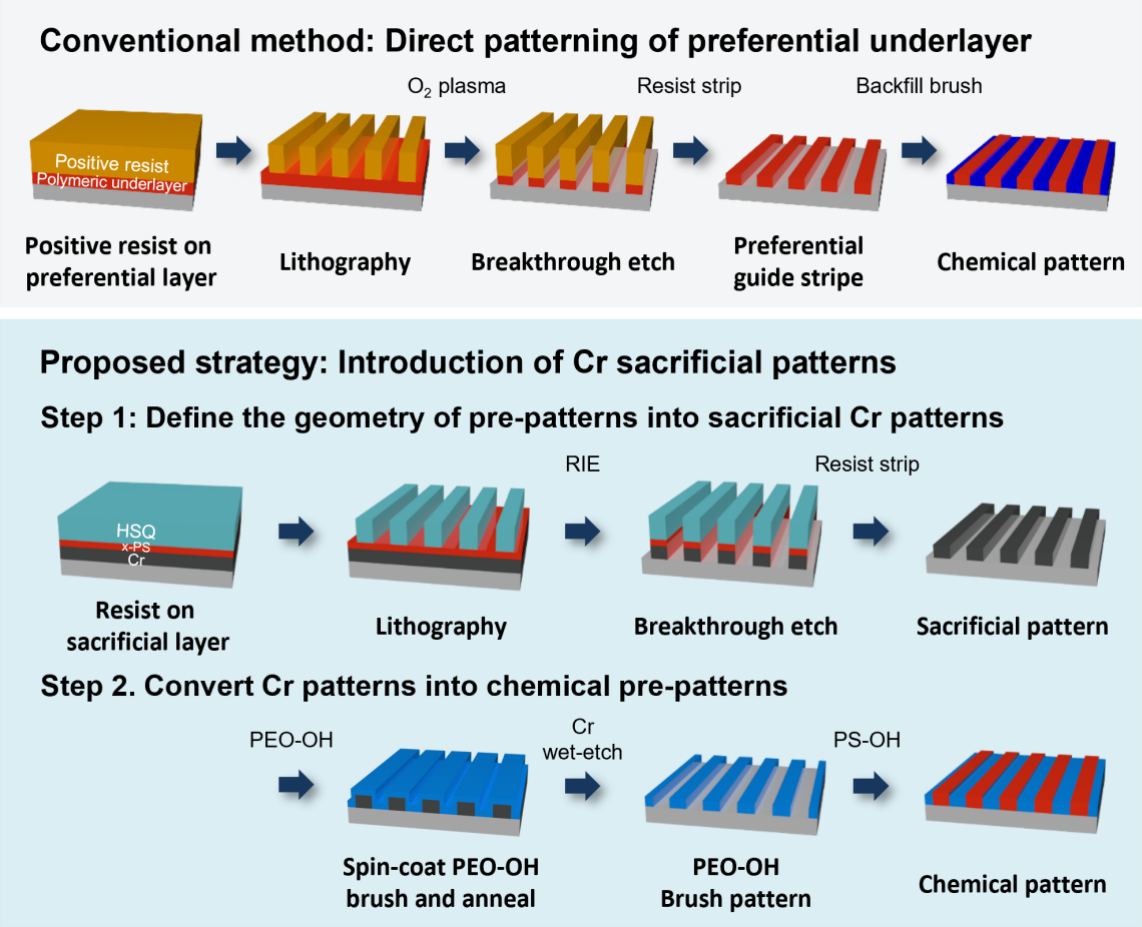

Figure 1. Schematic of chemical pattern formation process. The top section illustrates the conventional process flow utilizing positive tone resists. The bottom section shows the strategy proposed in this study, which uses negative tone resists.

Figure 2 demonstrates the initial step of the process involving the creation of sacrificial Cr patterns. The SEM images in the top row of Figure 2 show the HSQ patterns generated on the Cr and X-PS underlayer, where the bright lines represent the HSQ lines with a dark background of X-PS. We achieved line-and-space patterns at L_s of 38 nm down to 24 nm. HSQ patterns as small as 24 nm are comparable to the highest resolution of current EUV lithographic patterns of positive tone resists. Without the X-PS layer between the Cr and HSQ patterns, the HSQ patterns delaminated presumably due to their low adhesion to the

Cr surface (as shown in Supplementary Material Figure S2). Subsequently, the geometries of HSQ patterns were successfully transferred onto the Cr underlayer with RIE using a mixture gas of chlorine and oxygen. The SEM images in Figure 2d,e show the resulting sacrificial patterns with L_s of 38 nm and 26 nm. The critical dimensions of these patterns were 17 nm and 12 nm, respectively, falling within the optimal duty cycle of guide stripes for 1-to-1 DSA, which necessitates W_s within 30-65% of L_s[11]. However, for the L_s = 24 nm full-pitch patterns, the lines became wavy after RIE, presumably due to the high aspect ratio caused by the small line width (12 nm) compared to the total height of the stack (34 nm) (Figure 2e).

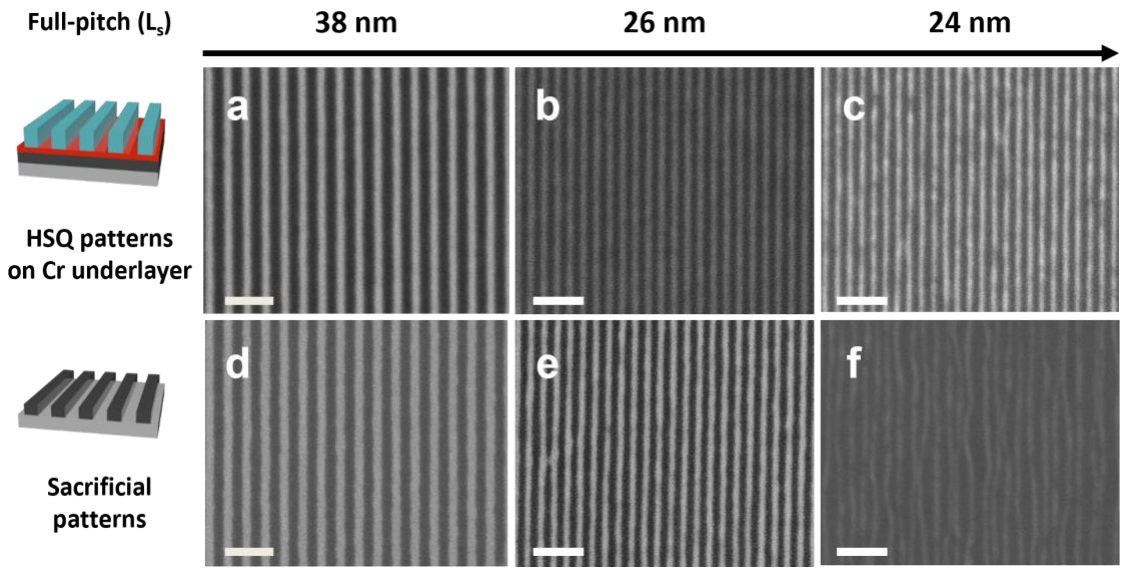

Figure 2. SEM images of HSQ patterns (top) and sacrificial patterns (bottom) at different full-pitch (L_s) values: (a) and (d) 38 nm; (b) and (e) 26 nm; (c) and (f) 24 nm. The scale bars are 100 nm.

To convert these Cr patterns into chemical patterns, our strategy aimed to orthogonally transform the areas occupied by Cr lines into non-polar PS-OH brushes and the interspatial areas into polar PEO-OH brushes. The effectiveness of the successive brush grafting involving Cr wet etching was assessed by measuring changes in total film thickness of deposited materials and WCA on two different blanket substrates (Figure 3a). A Cr-coated Si wafer represents Cr lines, and a bare Si wafer represents interspatial areas. Figure 3b shows the evolution of total film thickness after each step of the process. After piranha cleaning but before grafting the PEO-OH brush, the Cr-coated substrate had a thickness of 4.8 nm, while the Si substrate exhibited no deposited film. Upon grafting the PEO-OH brush (M_n = 4.2 kg/mol) onto the cleaned substrates, the total film thickness of each substrate increased by ~5 nm, indicating effective grafting of the PEO-OH brush. A significant difference between the two substrates was observed after treating them with a Cr wet etchant. The total film thickness of the Cr-coated substrate was reduced to ~1 nm, indicating the effective removal of both the Cr underlayer and PEO-OH brushes grafted on top. In contrast, the Si substrate exhibited only a minimal reduction in thickness, ~1 nm, suggesting that the PEO-OH brushes were retained. Subsequent grafting of the PS-OH (M_n = 2 kg/mol) brush resulted in a ~5 nm thick film on the Cr substrate, without noticeable changes in the film thickness on the Si substrate.

The orthogonal modification of each substrate with PS-OH and PEO-OH brushes was further confirmed by measuring the WCA (Figure 3c). Initially, both substrates exhibited a WCA of 0° before grafting the PEO-OH brush because they were cleaned with piranha solution. Following the grafting of the PEO-OH brush, both substrates had a WCA of ~30°, confirming effective grafting of the PEO-OH brush. Notably, the Cr blanket

substrate had a WCA of 0° after treating it with Cr wet etchant. This extremely low WCA reveals the exposure of Si surface to air by complete removal of the PEO brush. Subsequent grafting of the PS-OH brush onto this substrate resulted in a WCA of 90.1°, indicating successful modification with the non-polar PS-OH brush. In contrast, the WCA of Si blanket substrate remained at ~30° throughout the entire process, implying that this area retained the surface characteristics of the PEO-OH brush.

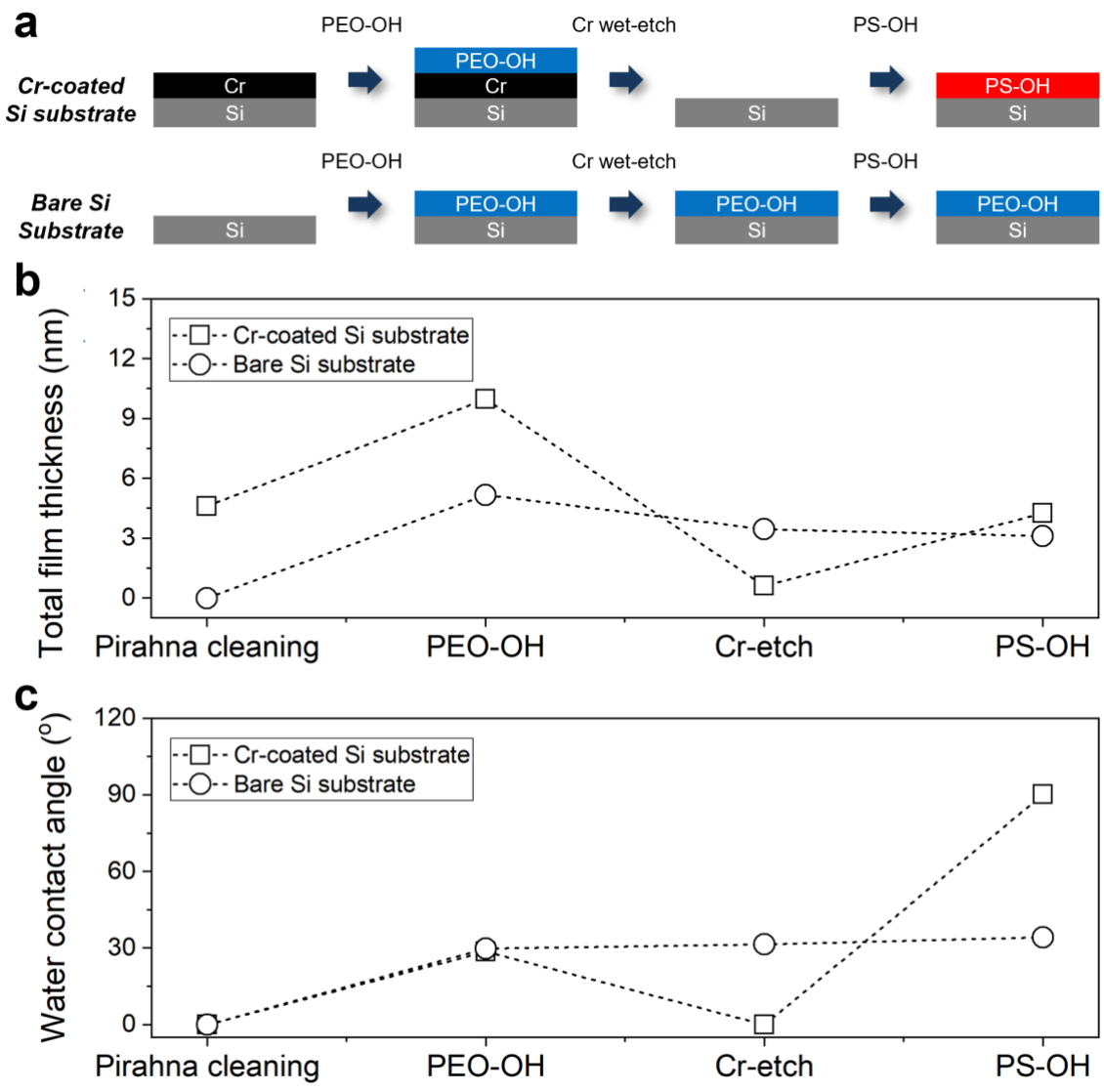

Figure 3. Changes in deposited materials on blanket substrates at each step of PEO-OH brush grafting, Cr wet-etching, and PS-OH brush grafting. (a) Schematic illustration. (b) Evolution of total film thickness. (c) Variation in water contact angle.

In addition to confirming the orthogonal modification of each substrate with PS-OH and PEO-OH, the wetting characteristics of PS-*b*-PMMA on each surface were validated with "island-hole" tests[23, 48]. In this experiment, a 1.25L_0-thick film of PS-*b*-PMMA (L_0 = 24 nm) was deposited onto each blanket substrate, both Cr-coated and bare Si, which had undergone PEO-OH brush grafting, Cr wet-etching, and PS-OH brush grafting. The PS-*b*-PMMA films were then annealed at 180 ℃ for 12 h to induce phase separation, resulting in a lamellar structure parallel to the substrate. Because the film thickness is not commensurate with an integer (n) multiple of L_0, the top surface of BCP film forms a "hole" or an "island" structure. Specifically, if the substrate prefers PS over PMMA, a 1.25 L_0 film forms islands on the top surface because this film generates a flat surface when the thickness is nL_0 due to the lower surface energy of PS compared to PMMA. Conversely, if the substrate prefers PMMA over PS, the film forms holes on the top surface[48]. Figure 4 presents the AFM images and corresponding height profiles of the assembled PS-*b*-PMMA film on each substrate. The surface of the BCP film on the processed Cr-coated substrate exhibited a $1L_0$ (24 nm) high island structure, indicating a PS-preferential surface (Figure 4a). In contrast, the bare Si substrate after process displayed $1L_0$ hole structures, indicating a PMMA-preferential substrate (Figure 4b). It is noted that PEO and PMMA have a negative Flory-Huggins interaction parameter, suggesting favorable interaction between the two polymers[49]. The island-hole tests confirmed that the Cr pattern and interspatial spaces were orthogonally modified with PS-OH and PEO-OH brushes, with each area preferring PS and PMMA, respectively.

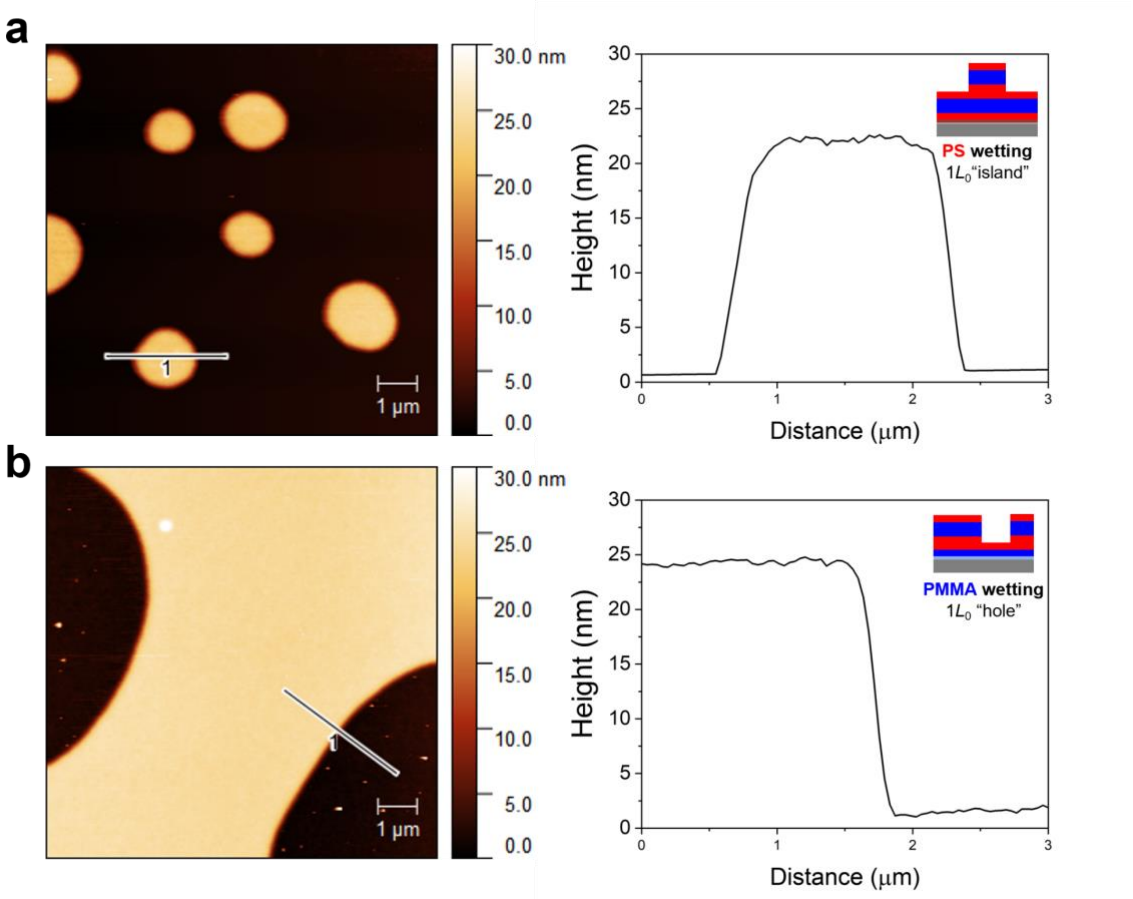

Figure 4. Island-hole test on a blanket substrate after chemical pattern fabrication. AFM images of PS-*b*-PMMA and cross-sectional profile along the lines: (a) Cr substrate; (b) Si substrate. The scale bars are 1 μm.

Finally, the sacrificial Cr patterns demonstrated in Figure 2 were converted into chemical patterns, and PS-*b*-PMMA copolymers with corresponding L_0 were assembled on top of them. Figure 5 shows the SEM images of BCP films assembled on each chemical pattern. As shown in the SEM images in Figure 5a,b, films of PS-*b*-PMMA with L_0 of 38 and 26 nm assembled into a perpendicular lamellar structure oriented to and registered with the underlying chemical patterns. The alignment of the materials was further clarified with fast Fourier transform analysis of the SEM images, showing clear peaks aligned

perpendicular to the direction of the line patterns. Despite the wavy Cr lines at 24 nm L_s, the assembled structure of PS-*b*-PMMA with 24 nm L_0 still aligned into straight lines, demonstrating the possibility of pattern rectification of chemical patterns generated by the proposed strategy through DSA (Figure 5c). However, on the patterns with L_s = 24 nm, significant defects and patchy areas were also observed, presumably due to the imperfections of the guide stripes.

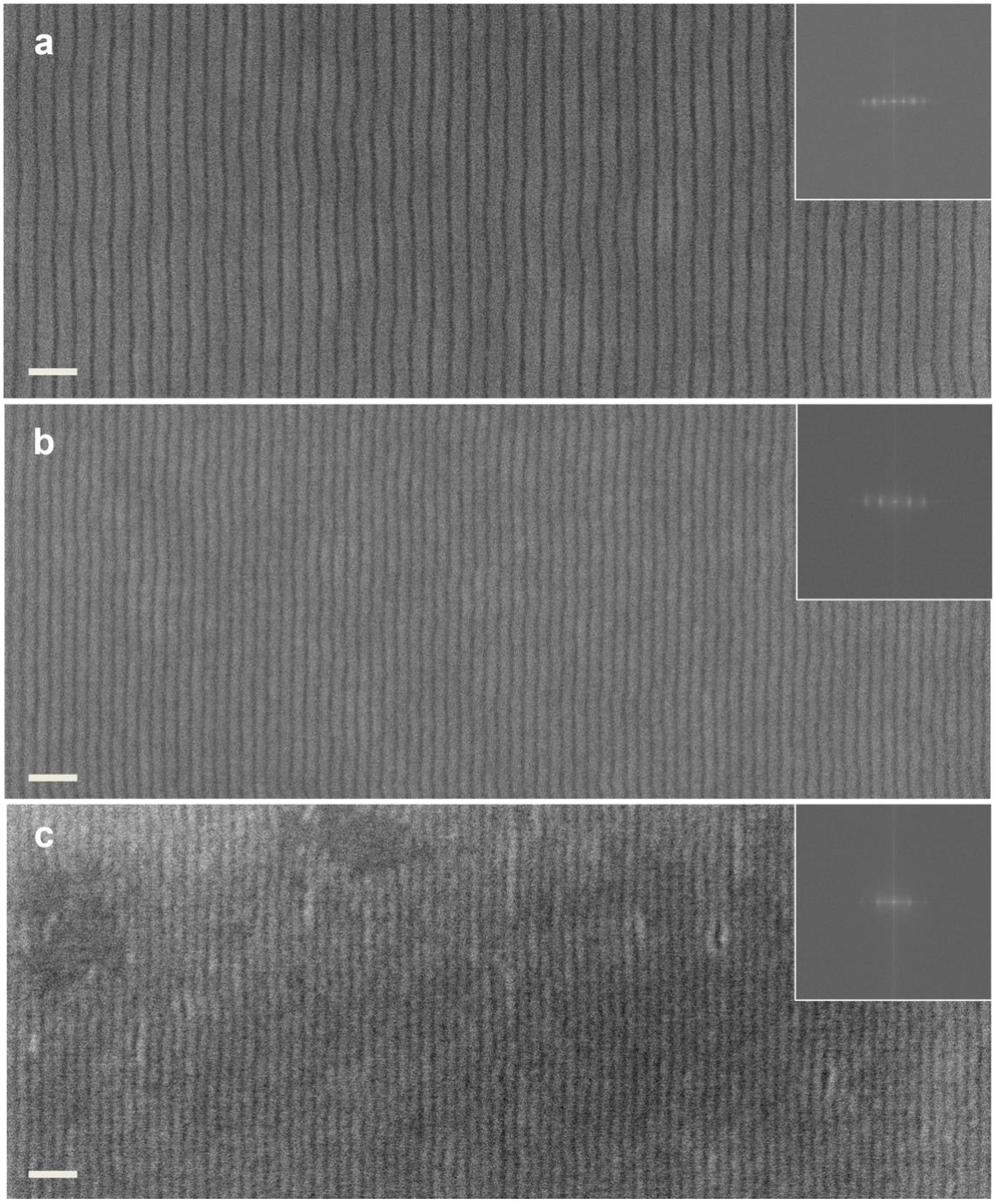

Figure 5. SEM images of PS-*b*-PMMA films assembled on chemically patterned surfaces. The natural period (L_0) of each polymer and the pattern period (L_s) are: (a) 38 nm; (b) 26 nm; and (c) 24 nm. The inset shows FFT spectrogram of each SEM image. The scale bars are 100 nm.

From a thermodynamic perspective, achieving a defect-free DSA pattern requires a substantial free energy gain with respect to any other state with a finite defect density[28, 50]. In this regard, a 1-to-1 chemical pattern with high chemical contrast provides the strongest guidance for defect-free patterns, affording a broad processing window, including higher tolerance for variations in L_s, duty cycle, and line roughness. For instance, even if L_s does not match L_0, sufficient chemical contrast can enable defect-free directed self-assembly[26]. The chemical pattern with strong chemical contrast not only reduces the synthetic efforts needed to create new BCP materials for targeted patterns but also lessens the stringent lithographic requirements for perfect pattern geometry. The robustness of chemical patterns was tested by assembling PS-*b*-PMMA with a 38 nm L_0 on top of chemical patterns with L_s of 36, 37, and 38 nm. As shown in the SEM images in Figure 6, all BCPs assembled according to the guiding patterns, resulting in structures with no noticeable defects. Notably, it has been reported that PS-*b*-PMMA on 1-to-1 chemical patterns composed of PS and PMMA brushes exhibited approximately 20% tolerance for L_s-L_0 mismatch[26]. Our study observed a tolerance window of about 5%; we plan to thoroughly investigate the full window in future studies.

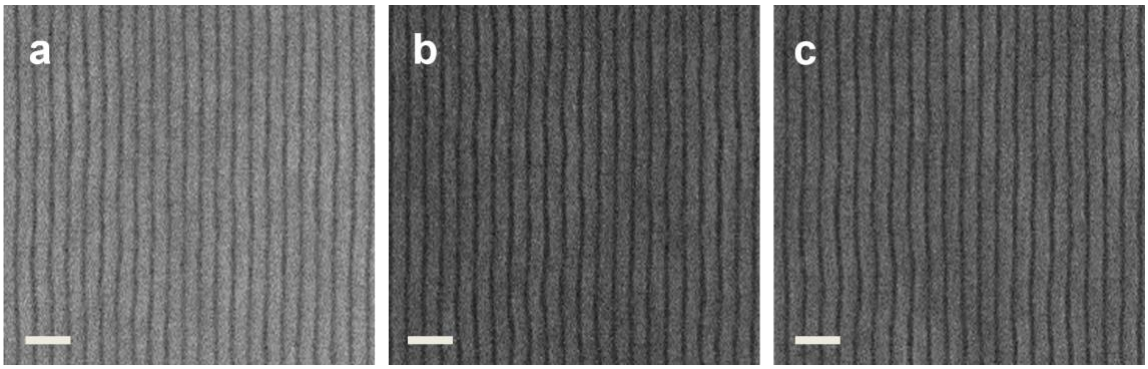

Figure 6. SEM images of PS-*b*-PMMA films with L_0 = 38.2 nm on chemically nanopatterned surfaces with the periods (L_s) of (a) 36 nm, (b) 37 nm, and (c) 38 nm. The scale bars are 100 nm.

While EUV lithography is now capable of printing features as small as those made by block copolymer self-assembly, DSA still offers promising opportunities to escape the RLS trade off by improving roughness, CD uniformity, edge placement error with a wider process window that can positively impact throughput and yield. The process flow presented in this work opens up a path to integrating the most promising negative-tone EUV resists with DSA. Current MOR patterns are recognized as an effective etch mask for pattern transfer into a variety of different underlayers[45], making them suitable for conversion into sacrificial patterns that are critical for our proposed strategy. For EUV plus DSA, the chemical patterns generated from MOR EUV patterns could not only enhance pattern quality through pattern rectification but also achieve sub-10 nm resolution through density multiplication with high χ BCPs by leveraging their highest resolution.

A promising variation on this strategy is to use different materials as a sacrificial underlayer instead of Cr, which can meet the design rules already described. As the feature sizes of interest to the lithography community continue to shrink, a very thin sacrificial

layer is required to prevent collapse during the pattern transfer process. In this context, using an ALD material could be advantageous, as it provides atomic precision in the thickness of the material, which is difficult to achieve with metallic thin films like Cr, typically deposited by physical vapor deposition. Additionally, choosing different sacrificial materials could improve compatibility of this process with various fabs.

IV. SUMMARY AND CONCLUSIONS

In this study, we introduced a new fabrication strategy for creating chemical patterns utilizing an e-beam pattern of HSQ, aimed at the integration of high-resolution MOR EUV patterns with DSA for pattern rectification. HSQ served as a model system for high-resolution MOR EUV patterns. By introducing a sacrificial pattern and converting it into polymer brush patterns, this method prevents the polymer brushes from being affected during the lithography and resist stripping steps, which often cause problems when integrating negative tone resists with conventional direct patterning of organic underlayers. Notably, the resulting chemical pattern excludes the negative tone resist itself, which will lead to effective pattern transfer of rectified patterns in DSA films. Initially, a sacrificial Cr pattern was generated by transferring the geometry of HSQ e-beam patterns via RIE. The sacrificial Cr pattern was then transformed into chemical patterns consisting of PS-OH and PEO-OH brush guide stripes by orthogonally modifying the Cr lines and interspatial areas through successive grafting of polymer brushes and wet-etching of Cr. The orthogonal modification was confirmed through thickness measurements and WCA analysis, with the preferential affinity of each area for the corresponding BCP domain further validated by the island-hole test. PS-*b*-PMMA assembled on these patterns formed well-ordered DSA structures down to 24 nm full-pitch, confirming the effectiveness of the chemical patterns with a tolerance window for mismatch between L_s and L_0 of ~5%. Given that MOR patterns can serve as effective etch masks for creating sacrificial Cr patterns, the process flow described in this work offers a pathway for rectifying imperfections in MOR EUV patterns through DSA.

SUPPLEMENTARY MATERIAL

The supplementary material includes additional SEM images related to the PS-*b*-PMMA used in this study, assembled on non-patterned neutral substrates (Figure S1), and the HSQ e-beam patterns on Cr underlayer with/without X-PS (Figure S2).

ACKNOWLEDGMENTS

This work was supported as part of the Center for High Precision Patterning Science (CHiPPS), an Energy Frontier Research Center funded by the U.S. Department of Energy, Office of Science, Basic Energy Sciences at Lawrence Berkeley National Laboratory under contract # DE-AC02-05CH11231. SEM and AFM were performed at the MRSEC Shared User Facilities at the University of Chicago (NSF DMR-1420709). E-beam lithography and reactive ion etching, physical vapor deposition using the e-beam evaporator were conducted at the Pritzker Nanofabrication Facility of the Pritzker School of Molecular Engineering at the University of Chicago, which receives support from Soft and Hybrid Nanotechnology Experimental (SHyNE) Resource (NSF ECCS-1542205), a node of the National Science Foundation's National Nanotechnology Coordinated Infrastructure.

CONFLICTS OF INTEREST

The authors have no conflicts to disclose.

DATA AVAILABILITY

Data available in article or supplementary material.

REFERENCES

(1) J. Van Schoot, E. van Setten, K. Troost, S. Lok, J. Stoeldraijer, R. Peeters, J. Benschop, J. Zimmerman, P. Graeupner and L. Wischmeier, Extreme Ultraviolet (EUV) Lithography XI, **11323**, 15-24 (2020).

(2) O. Versolato, J. Sheil, S. Witte, W. Ubachs and R. Hoekstra, Journal of Optics, **24**, 054014 (2022).

(3) H. J. Levinson, Japanese Journal of Applied Physics, **61**, SD0803 (2022).

(4) H. Tang, J. C. Shearer, L. L. Cheong, N. A. Saulnier, S. A. Sieg, K. Petrillo, A. Metz and J. C. Arnold, Journal of Photopolymer Science and Technology, **28**, 13-16 (2015).

(5) C. Bencher, Y. Chen, H. Dai, W. Montgomery and L. Huli, Optical Microlithography XXI, **6924**, 1440-1446 (2008).

(6) C. K. Ober, H. Xu, V. Kosma, K. Sakai and E. P. Giannelis, Extreme Ultraviolet (EUV) Lithography IX, **10583**, 15-27 (2018).

(7) S. Kruger, C. Higgins, C. Gallatin and R. Brainard, Journal of Photopolymer Science and Technology, **24**, 143-152 (2011).

(8) G. M. Gallatin, P. Naulleau and R. Brainard, Advances in Resist Materials and Processing Technology XXIV, **6519**, 387-396 (2007).

(9) C. Higgins, A. Antohe, G. Denbeaux, S. Kruger, J. Georger and R. Brainard, Alternative Lithographic Technologies, **7271**, 1118-1129 (2009).

(10) R. Gronheid, A. V. Pret, B. Rathsack, J. Hooge, S. Scheer, K. Nafus, H. Shite and J. Kitano, Advances in Resist Materials and Processing Technology XXVII, **7639**, 203-211 (2010).

(11) E. W. Edwards, M. Müller, M. P. Stoykovich, H. H. Solak, J. J. de Pablo and P. F. Nealey, Macromolecules, **40**, 90-96 (2007).

(12) M. P. Stoykovich, K. C. Daoulas, M. Muller, H. Kang, J. J. de Pablo and P. F. Nealey, Macromolecules, **43**, 2334-2342 (2010).

(13) S. Ji, L. Wan, C.-C. Liu and P. F. Nealey, Progress in Polymer Science, **54**, 76-127 (2016).

(14) S. M. Park, M. P. Stoykovich, R. Ruiz, Y. Zhang, C. T. Black and P. F. Nealey, Advanced Materials, **19**, 607-611 (2007).

(15) M. W. Matsen and F. S. Bates, Macromolecules, **29**, 1091-1098 (1996).

(16) A. Semenov, Macromolecules, **26**, 6617-6621 (1993).

(17) L. Verstraete, H. S. Suh, J. Van Bel, P. H. Timi, R. Vallat, P. Bezard, J. Vandereyken, M. Beggiato, A.-H. Tamaddon and C. Beral, Novel Patterning Technologies 2023, **12497**, 135-144 (2023).

(18) R. Ruiz, H. Kang, F. A. Detcheverry, E. Dobisz, D. S. Kercher, T. R. Albrecht, J. J. de Pablo and P. F. Nealey, Science, **321**, 936-939 (2008).

(19) L. Verstraete, H. S. Suh, J. Van Bel, B.-U. Bak, S. E. Kim, R. Vallat, P. Bezard, M. Beggiato and C. Beral, Novel Patterning Technologies 2024, **12956**, 116-124 (2024).

(20) F. Gstrein, Novel Patterning Technologies 2021, **11610**, 116100J (2021).

(21) L. Wan, R. Ruiz, H. Gao, K. C. Patel, T. R. Albrecht, J. Yin, J. Kim, Y. Cao and G. Lin, ACS nano, **9**, 7506-7514 (2015).

(22) H. Tsai, H. Miyazoe, A. Vora, T. Magbitang, N. Arellano, C.-C. Liu, M. J. Maher, W. J. Durand, S. J. Dawes and J. J. Bucchignano, Advances in Patterning Materials and Processes XXXIII, **9779**, 128-134 (2016).

(23) H. Feng, M. Dolejsi, N. Zhu, S. Yim, W. Loo, P. Ma, C. Zhou, G. S. Craig, W. Chen and L. Wan, Nature Materials, **21**, 1426-1433 (2022).

(24) J. Wandell, K. Gorman, B. Alperson, D. Baskaran, M. S. Rahman, J. Kim, S. Michlik, Y. Her and S. Miyazaki, Novel Patterning Technologies 2024, **12956**, 111-115 (2024).

(25) S. Ouk Kim, H. H. Solak, M. P. Stoykovich, N. J. Ferrier, J. J. De Pablo and P. F. Nealey, Nature, **424**, 411-414 (2003).

(26) E. W. Edwards, M. F. Montague, H. H. Solak, C. J. Hawker and P. F. Nealey, Advanced Materials, **16**, 1315-1319 (2004).

(27) C.-C. Liu, E. Han, M. S. Onses, C. J. Thode, S. Ji, P. Gopalan and P. F. Nealey, Macromolecules, **44**, 1876-1885 (2011).

(28) C.-C. Liu, A. Ramírez-Hernández, E. Han, G. S. Craig, Y. Tada, H. Yoshida, H. Kang, S. Ji, P. Gopalan and J. J. De Pablo, Macromolecules, **46**, 1415-1424 (2013).

(29) L. Li, X. Liu, S. Pal, S. Wang, C. K. Ober and E. P. Giannelis, Chemical Society Reviews, **46**, 4855-4866 (2017).

(30) C. K. Ober, F. Käfer and C. Yuan, Polymer, **280**, 126020 (2023).

(31) J. Stowers, J. Anderson, B. Cardineau, B. Clark, P. De Schepper, J. Edson, M. Greer, K. Jiang, M. Kocsis and S. Meyers, Advances in Patterning Materials and Processes XXXIII, **9779**, 977904 (2016).

(32) E. Buitrago, R. Fallica, D. Fan, T. S. Kulmala, M. Vockenhuber and Y. Ekinci, Microelectronic Engineering, **155**, 44-49 (2016).

(33) S. Enomoto, K. Machida, M. Naito and T. Kozawa, International Conference on Extreme Ultraviolet Lithography 2022, **12292**, 101-105 (2022).

(34) C. D. Needham, U. Welling, A. Narasimhan, P. De Schepper, L. McQuade, M. Kocsis, L. S. Melvin III, J. Stowers and S. T. Meyers, Advances in Patterning Materials and Processes XLI, **12957**, 243-260 (2024).

(35) M. J. Maher, C. T. Rettner, C. M. Bates, G. Blachut, M. C. Carlson, W. J. Durand, C. J. Ellison, D. P. Sanders, J. Y. Cheng and C. G. Willson, ACS applied materials & interfaces, **7**, 3323-3328 (2015).

(36) H. S. Suh, L. Verstraete, J. Van Bel, P. Bézard, G. Mannaert, J. U. Lee, S. Wang, I. Pollentier and A. Rathore, Novel Patterning Technologies 2022, PC1205402 (2022).

(37) M. Suzuki, Y. Kim, Y. Her, H. Wu, K. Si, M. M. Maturi, P. H. Fackler, M. Moinpour, R. Dammel and Y. Cao, Advances in Patterning Materials and Processes XL, **12498**, 192-203 (2023).

(38) C.-C. Liu, P. F. Nealey, Y.-H. Ting and A. E. Wendt, Journal of Vacuum Science & Technology B: Microelectronics and Nanometer Structures Processing, Measurement, and Phenomena, **25**, 1963-1968 (2007).

(39) T. Thurn-Albrecht, R. Steiner, J. DeRouchey, C. M. Stafford, E. Huang, M. Bal, M. Tuominen, C. J. Hawker and T. P. Russell, Advanced Materials, **12**, 787-791 (2000).

(40) Y.-C. Tseng, Q. Peng, L. E. Ocola, J. W. Elam and S. B. Darling, The Journal of Physical Chemistry C, **115**, 17725-17729 (2011).

(41) Q. Peng, Y.-C. Tseng, S. B. Darling and J. W. Elam, ACS nano, **5**, 4600-4606 (2011).

(42) E. Drockenmuller, L. Y. T. Li, D. Y. Ryu, E. Harth, T. P. Russell, H. C. Kim and C. J. Hawker, Journal of Polymer Science Part a-Polymer Chemistry, **43**, 1028-1037 (2005).

(43) F. Aydinoglu, H. Yamada, R. K. Dey and B. Cui, Langmuir, **33**, 4981-4985 (2017).

(44) R. K. Dey and B. Cui, Nanotechnology, **24**, 245302 (2013).

(45) M. Mao, F. Lazzarino, P. De Schepper, D. De Simone, D. Piumi, V. Luong, F. Yamashita, M. Kocsis and K. Kumar, Advances in Patterning Materials and Processes XXXIV, **10146**, 110-118 (2017).

(46) M. Mohammad, S. Dew, S. Evoy and M. Stepanova, Microelectronic engineering, **88**, 2338-2341 (2011).

(47) Y. Ekinci, H. H. Solak, C. Padeste, J. Gobrecht, M. P. Stoykovich and P. F. Nealey, Microelectronic engineering, **84**, 700-704 (2007).

(48) T. P. Russell, G. Coulon, V. Deline and D. Miller, Macromolecules, **22**, 4600-4606 (1989).

(49) H. Ito, T. P. Russell and G. Wignall, Macromolecules, **20**, 2213-2220 (1987).

(50) L. Wan, R. Ruiz, H. Gao and T. R. Albrecht, ACS nano, **11**, 7666-7673 (2017).